JOURNAL OF CATALYSIS **175,** 252–268 (1998)
ARTICLE NO. CA982003

Microcalorimetric, FTIR, and DFT Studies of the Adsorption of Methanol, Ethanol, and 2,2,2-Trifluoroethanol on Silica

M. A. Natal-Santiago and J. A. Dumesic[1]

Department of Chemical Engineering, University of Wisconsin, Madison, Wisconsin 53706

Received September 2, 1997; revised December 31, 1997; accepted January 5, 1998

The adsorption and reaction of methanol, ethanol, and 2,2,2-trifluoroethanol on silica at 300 K were studied by combining microcalorimetric and infrared spectroscopic (FTIR) measurements with quantum-chemical calculations based on density-functional theory (DFT). Methanol, ethanol, and 2,2,2-trifluoroethanol adsorb molecularly on silica via formation of hydrogen bonds, with initial heats of interaction of 78, 100, and 90 (± 2) kJ/mol, respectively. Methanol and 2,2,2-trifluoroethanol adsorbed on silica can be removed by evacuation at 473 K, whereas small amounts (∼5 μmol/g) of ethoxy species remain on silica after evacuation at 573 K. Two pathways are considered for the alkoxylation of silica: one pathway involving protonation of the adsorbed alcohol by surface hydroxyls and the other involving protonation and subsequent cleavage of Si–OH bonds or SiO–Si bridges by the adsorbed alcohol. The activation energies for the formation of methoxy, ethoxy, and 2,2,2-trifluoroethoxy species via the first pathway are estimated to be 309, 285, and 321 kJ/mol, respectively, whereas activation energies for the second pathway are estimated to be 117, 117, 138 kJ/mol. The high activation barrier for the first pathway is caused by the localization of positive charge in the alkyl group of the transition state, which is made difficult by the weak acidity of silica and the instability of methyl, ethyl, and 2,2,2-trifluoroethyl carbenium ions. The second proposed mechanism is controlled mainly by the acid strength of the alcohols and the extent of delocalization of electron density in the four-member ring present in the transition states.

Key Words: **methanol; ethanol; trifluoroethanol; adsorption; silica; microcalorimetry; density-functional theory (dft); Fourier-transform infrared spectroscopy (ftir).**

INTRODUCTION

The adsorption and reaction of alcohols on oxide catalysts are important in the industrial production of alkenes, esters, ethers, aldehydes, and alkylamines (1). In addition, methanol and ethanol are used in the production of blending compounds for reformulated gasoline (2). Fluorinated alcohols such as 2,2,2-trifluoroethanol have been used to modify the acidity of oxides to improve their catalytic activity for cracking and isomerization reactions of hydrocarbons (3, 4).

Various studies of alcohol adsorption on acidic oxides have been conducted, particularly that of methanol (5–19) and ethanol (20–27) adsorption on silica. In general, interactions between the adsorbed alcohol and oxide surface depend on the pre-treatment of silica. For example, the adsorption of alcohols via hydrogen-bonding interactions with silanol groups and siloxane bridges is predominant on samples outgassed at temperatures below 623 K (10, 17–19). For samples of silica pretreated at temperatures higher than 623 K (10, 17–19, 28–36), "strained" siloxane bridges are generated that facilitate the dissociative adsorption of alcohols to produce alkoxy species, which desorb only at temperatures higher than 873 K. The formation of alkoxy species has been proposed to occur on both silanol groups and siloxane bridges, but preferentially on the latter type of sites. While the adsorption and reaction of alcohols on silica have been considered theoretically (5–7, 20, 32), no study to our knowledge has examined the corresponding transition states that control the rate of alkoxylation of silica.

In the present work, we have studied the adsorption of methanol, ethanol, and 2,2,2-trifluoroethanol on silica. We have chosen to study silica because this oxide is generally considered to be a weak acid, and we will thus address the origin of the low reactivity of this weakly acidic oxide. Moreover, we have chosen to study the interactions of alcohols with silica pretreated such that "strained" siloxane bridges are not present on the surface in significant amounts, thus allowing for the study of alkoxylation processes via interactions of the adsorbed alcohols with surface hydroxyls and siloxane bridges only. Heat-flow microcalorimetry was used to measure the heats of interaction of methanol, ethanol, and 2,2,2-trifluoroethanol with silica; Fourier-transform infrared spectroscopy (FTIR) techniques were employed to determine the nature of the surface species; and, quantum chemical-calculations were performed on the basis of density-functional theory (DFT) to probe the potential energy surfaces (PES) for the interaction of the aforementioned alcohols with silica. We will show that the formation of alkoxy species via protonation of molecularly adsorbed

[1] To whom correspondence should be addressed.

0021-9517/98 $25.00

alcohols by surface hydroxyls is a highly activated process, which depends not only on the acid strength of the oxide but also on the stability of the carbenium ion formed by removal of the hydroxyl group from the alcohol. In contrast, the activation barrier is significantly lower for the formation of alkoxy species via protonation and subsequent cleavage of Si–OH bonds or SiO–Si bridges by the adsorbed alcohol. In this case, the activation process depends mainly on the acid strength of the adsorbed alcohol and the extent of delocalization of electron density in the four-member ring present in the transition state.

METHODOLOGY

Microcalorimetric measurements were performed using a Tian–Calvet, heat-flow microcalorimeter (Seteram C80) connected to a calibrated dosing system equipped with a capacitance manometer (Baratron, MKS). A detailed description of the apparatus and techniques may be found elsewhere (37, 38). Prior to each experiment, 500–600 mg of Cab–O–Sil (∼380 m^2/g) was outgassed in vacuum (∼1 mPa) for 2 h at 600 K and subsequently cooled to room temperature. The microcalorimetric cells were then placed in the thermal block of the calorimeter, and measurements were initiated after the cells had equilibrated with the calorimeter at 300 K (typically overnight). Methanol (Aldrich, 99.9%), ethanol (Pharmco, 200° proof), and 2,2,2-trifluoroethanol (Aldrich, 99.5%) were purified by freeze-pump-thaw cycles.

Infrared absorption spectra were collected at room temperature using a Mattson Galaxy 5020, FTIR spectrometer with a resolution of 2 cm^{-1}. Samples of Cab–O–Sil (10–20 mg) were pressed into self-supporting wafers (∼12 mm diameter) at a pressure of ∼60 MPa. Prior to measurements, samples were outgassed in vacuum for 2 h at 600 K inside a cell equipped with CaF_2 windows. After collecting the spectrum for silica, a specific pressure of alcohol was admitted into the cell and spectra for the alcohol adsorbed on silica were collected. To investigate the reversibility of the adsorption process, spectra were collected after outgassing overnight at room temperature, for 2 h at 473 K, and for 2 h at 573 K.

Quantum-chemical calculations were performed on the basis of DFT, using the three-parameter functional B3P86 (39) along with the basis sets 6-31+G* and 3-21+G*, as specified below (40). Detailed information about the theory can be found elsewhere (41, 42). The calculations were performed using the software package *Gaussian 94*® (43) on IBM SP2 and DEC Alpha computers. Structural parameters were determined by optimizing to stationary points on the PES of the corresponding stoichiometry using the Berny algorithm and redundant internal coordinates (44). For computational simplicity, hydrogen-terminated silanol groups and siloxane bridges were chosen to model the surface of silica in studies of ethanol and 2,2,2-trifluoroethanol adsorption. The error introduced by hydrogen-termination of the clusters was estimated by comparisons of analogous calculations performed for methanol interacting with hydrogen- and hydroxyl-terminated clusters. These models have been shown to be adequate for the quantitative description of one- and twofold hydrogen-bonding interactions on silica hydroxyls (5–7). Computations with hydrogen-terminated clusters were performed using the basis set 6-31+G*, whereas the 3-21+G* basis set was used to model the terminating hydroxyl groups, as needed.

To investigate the rate at which alkoxy species form on silica hydroxyls and siloxane bridges, the corresponding transition states were located on the PES. The location of transition states proceeded according to a STQN method, which uses a linear or quadratic synchronous transit approach to get closer than an initial guess to the quadratic region of the PES, followed by a quasi-Newton or eigenvalue-following algorithm to complete the optimization (45). These optimizations were performed using redundant internal coordinates. Optimization criteria consisted of maximum and root-mean-squared forces of less than 22 and 15 J/mol-pm, respectively. The molecular structures resulting from the optimizations were classified as local minima or transition states on the PES by calculating the Hessian (force-constant) matrix analytically. For local minima, the eigenvalues of the Hessian matrix were all positive, whereas for transition states only one eigenvalue was negative (40). The vibrational frequencies obtained from the analysis of force constants were used further without scaling, unless specified otherwise, to estimate the thermochemical properties of the clusters of interest at 298 K. To verify that the transition states correspond to the chemical reactions of interest, intrinsic reaction coordinate (IRC) calculations were performed using mass-weighted internal coordinates to follow the reaction paths in forward and reverse directions from the first-order saddle points (46, 47), thus resulting in the reaction coordinate being expressed in units of length $\cdot \sqrt{\text{mass}}$ (48).

RESULTS AND DISCUSSION

Microcalorimetric Measurements

Microcalorimetric results for the adsorption of methanol, ethanol, and 2,2,2-trifluoroethanol (hereafter named tfetoh) are shown in Fig. 1 in the form of differential heat of adsorption versus alcohol coverage. For convenience, the differential heat of adsorption has been defined as the negative of the differential change in enthalpy for the adsorption process. The trends included in Fig. 1 were obtained by differentiating polynomial fits of the integral heat versus adsorbate coverage. The initial heat of methanol adsorption on silica is 78 ± 2 kJ/mol. This value is in agreement

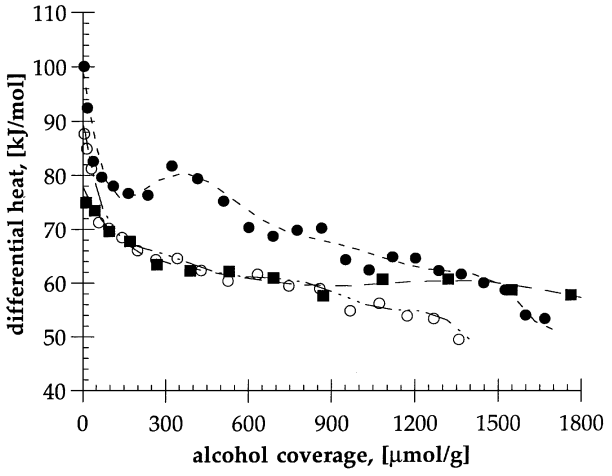

FIG. 1. Differential heat versus surface coverage for the adsorption of methanol (■), ethanol (●), and 2,2,2-trifluoroethanol (○) on silica at 300 K. The trends (dashed lines) included were obtained by differentiating polynomial fits of the integral heat curves.

with previous investigations of methanol adsorption on silicalite (23) and pyrogenic silica (49), where initial heats of 80–90 kJ/mol were reported. As the methanol coverage increases, the heat of adsorption decreases monotonically until a coverage of ~250 μmol/g. At higher coverages, the heat of adsorption is nearly constant at 60 ± 4 kJ/mol. These measurements are in agreement with previous investigations (49, 50) in which values of 60–65 kJ/mol were reported for methanol adsorption on silica at moderate to high coverages. The shape of the differential heat curve suggests the existence of at least two modes of methanol adsorption, that is, different modes of adsorption at coverages above and below ~250 μmol/g.

The initial heat of ethanol adsorption on silica is 100 ± 2 kJ/mol. As the coverage increases, the heat of adsorption decreases and may pass through a local maximum at a coverage of 320 μmol/g. The presence of a local maximum in the heat of alcohol adsorption on silica and silicalite has been observed previously (18, 23, 26), being interpreted as the onset of lateral hydrogen-bonding interactions between neighboring alcohol molecules. At coverages higher than 320 μmol/g, the heat of adsorption decreases monotonically, reaching 54 kJ/mol at a coverage of 1600 μmol/g. The shape of the differential heat curve suggests the existence of at least two modes of ethanol adsorption, with different modes of adsorption at coverages above and below ~120 μmol/g. These measurements are in agreement with previous studies performed for the adsorption of ethanol on silica (22) and silicalite (23), where initial heats of 96–100 kJ/mol have been reported, with heats of 46–70 kJ/mol at coverages higher than 400 μmol/g.

The initial heat of tfetoh adsorption on silica is 90 ± 2 kJ/mol. The differential heat for tfetoh adsorption approaches that for methanol adsorption for the range of coverages from 100 to 900 μmol/g. The shape of the differential heat curve suggests the presence of at least two modes of tfetoh adsorption, with different modes of adsorption at coverages above and below ~100 μmol/g. Previous spectroscopic investigations of the adsorption of tfetoh on isolated silica hydroxyls have suggested an average hydrogen-bond energy of 28–33 kJ/mol (4). According to this result, our initial heat of tfetoh adsorption would correspond to surface species bound to silica and/or perhaps to each other by three hydrogen bonds.

The adsorption of methanol, ethanol, and tfetoh on silica at low to moderate temperatures is believed to involve more than one hydrogen bond between the alcohol and surface hydroxyls and/or siloxane bridges, each bond having an average strength of 22–28 kJ/mol (18, 19). On the basis of this view, the formation of three hydrogen bonds between surface alcohols and silica, and/or perhaps between neighboring alcohol molecules, is expected at low to moderate coverages (18, 19), whereas two hydrogen bonds may be formed at moderate to high coverages. Our initial heats of adsorption thus suggest average hydrogen-bond strengths of approximately 26, 33, and 30 kJ/mol for adsorption of methanol, ethanol, and tfetoh, respectively. It appears that fluorination of the methyl group in ethanol results in a slight decrease of the hydrogen bonding strength of the alcohol, most likely due to the inductive effect of electron-withdrawing CF_3 groups.

FTIR Measurements

Methanol adsorption. Infrared absorption spectra were collected at room temperature for silica, gaseous methanol, and methanol adsorbed on silica, and these spectra were subtracted to produce the difference-spectra in Fig. 2a. The 1300–2000 cm^{-1} region of the methanol absorption spectra is included in Fig. 3. The bands observed in these spectra are summarized in Table 1 and compared with DFT predictions from this work for adsorbed methanol (discussed in the next section) and literature data for gaseous methanol. The spectrum in Fig. 2a(i) was collected at a methanol pressure of 28 Pa, which corresponds to a surface coverage of ~30 μmol/g. In general, C–H stretching and bending modes of vibration are affected slightly, while the perturbation of O–H stretching and C–O–H bending modes is more evident. In particular, the antisymmetric C–H stretching and bending modes are shifted to lower wavenumbers by 5–10 cm^{-1}, while C–O–H bending is shifted to higher wavenumbers by 28 cm^{-1}. The alcohol ν(OH), $\nu_s(CH_3)$, and $\delta_s(CH_3)$ modes are shifted by −346, 10, and −5 cm^{-1}, respectively.

The bands observed at 2928 and 1708 cm^{-1} in the spectra of Figs. 2a and 3 cannot be assigned with certainty. However, it has been suggested (10) that the band at 2928 cm^{-1} corresponds to overtones or combinations of methyl deformation modes. The assignment of the band at 1708 cm^{-1} is

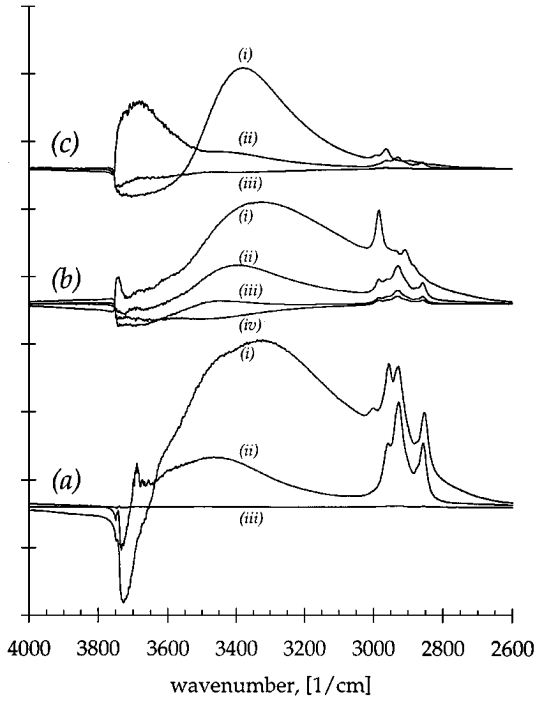

FIG. 2. Difference FTIR spectra for (a) methanol, (b) ethanol, and (c) 2,2,2-trifluoroethanol adsorbed on silica at room temperature. (a) Methanol spectra: (i) ~30 μmol/g on silica, (ii) after subsequent evacuation at room temperature, and (iii) after subsequent evacuation at 473 K. (b) Ethanol spectra: (i) ~40 μmol/g on silica, (ii) after subsequent evacuation at room temperature, (iii) after subsequent evacuation at 473 K, and (iv) after subsequent evacuation at 573 K. (c) Trifluoroethanol spectra: (i) ~130 μmol/g on silica, (ii) after subsequent evacuation at room temperature, and (iii) after subsequent evacuation at 473 K. The vertical scale has been divided in 0.5 absorbance units.

less clear, but it may involve a combination of modes, perhaps involving ν(CO), that becomes active at moderate to high coverages or at the onset of lateral hydrogen-bonding interactions.

To investigate the reversibility of methanol adsorption on silica, the sample was outgassed overnight in vacuum and infrared absorption spectra collected. The corresponding difference-spectrum is included in Fig. 2a(ii), from which it can be seen that some methanol (~20 μmol/g) remains on the surface after evacuation at room temperature. The (negative) band observed at 3750 cm^{-1} can be attributed to interactions of methanol with isolated silanol groups, given the correspondence of this wavenumber with that extensively assigned to ν(OH) of isolated silanol groups. The sample was subsequently outgassed at 473 K for 2 h and infrared absorption spectra collected. The corresponding difference-spectrum is included in Fig. 2a(iii), from which it can be concluded that all adsorbed methanol can be removed by evacuation at 473 K. These findings are in agreement with previous reports that an outgassing temperature of 473 K is required for the complete removal of molecularly-adsorbed methanol (18, 19). We may conclude that methoxy species were not formed on silica in our study, since it has been reported (17) that these species would not have been removed by evacuation at the conditions of our study (that is, at temperatures below 873 K).

To study the effect of surface coverage on the mode of methanol adsorption, infrared absorption spectra were collected of silica for three different coverages of methanol. The 1300–2000 cm^{-1} region of the difference-spectra is included in Fig. 3. As the coverage of methanol increases from approximately 30 to 600 μmol/g, the band at 1708 cm^{-1} grows while a triplet develops in the region where δ(COH) modes are observed, that is, bands at 1366, 1380, and 1394 cm^{-1}. This triplet is present after evacuation at room temperature, as shown in Fig. 3(vi), although the relative intensities change. This triplet may be caused by methanol hydroxyls in three or more different environments, as suggested in structural models reported previously (5–7). Hence, on the basis of this and the preceding observations, the presence of methanol molecules bound by two and three hydrogen bonds is suggested at low coverages, with perhaps the formation of polymeric chains even at low coverages. This interpretation is consistent with shifts of the δ(COH) band relative to isolated methanol observed previously for methanol dimers and oligomers in Argon matrices (51, 52).

Ethanol adsorption. Infrared absorption spectra were collected at room temperature for silica, gaseous ethanol,

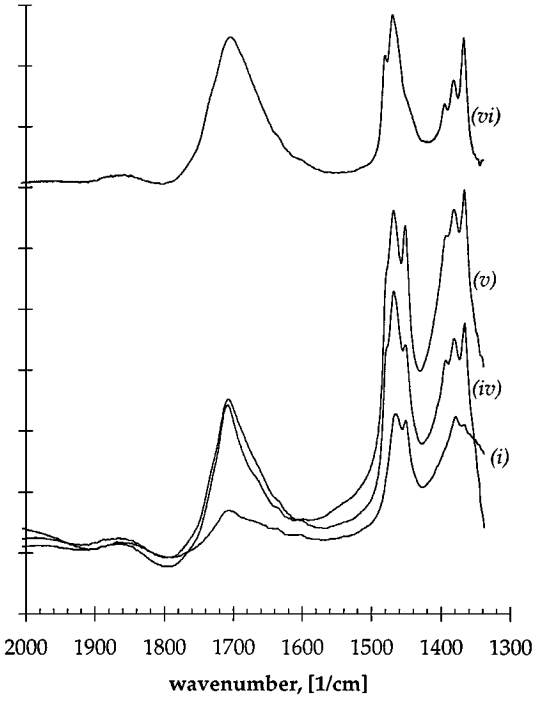

FIG. 3. Difference FTIR spectra for (i) ~30 μmol/g, (iv) ~300 μmol/g, and (v) ~600 μmol/g of methanol adsorbed on silica at room temperature, and (vi) after evacuation at room temperature of sample (v). The vertical scale has been divided in 0.1 absorbance units.

TABLE 1

Wavenumbers (cm^{-1}) for the Fundamental Modes of Vibration of Methanol in the Gas Phase (C_s Point Group) and Adsorbed Molecularly and Dissociatively (Methoxy) on Silica at Room Temperature

	Experimental			DFT prediction[b]				
Description	Gas[a]	Adsorbed 2a(i) & 3(i)	Adsorbed 2a(ii)	Gas	Adsorbed 4(a)	Adsorbed 4(b)	Adsorbed 6(a)	Methoxy 7(c)
ν(OH)	3682	3336[c]	3466, 3690[c]	3662	3661	3693	3564	—
$\nu''_{as}(CH_3)$	3005	3000		3039	3059	3018	3046	3043
$\nu'_{as}(CH_3)$	2962	2954	2958	2958	3001	2936	2984	3003
$2\delta''_{as}(CH_3)$		2928	2926					
$\nu_s(CH_3)$	2844	2854	2856	2906	2935	2890	2924	2930
2ν(CO)	2053							
		1708	1702					
$\delta''_{as}(CH_3)$	1474			1469	1467	1472	1469	1468
$\delta''_{as}(CH_3)$	1466	1466	1464	1458	1460	1458	1459	1460
$\delta'_{as}(CH_3)$	1455	1450		1438	1437	1438	1437	1439
δ'(COH)	1340	1378	1366, 1380	1320	1325	1377	1343	—
$\rho''_r(CH_3)$	1150			1135	1139	1137	1138	1173
$\rho'_r(CH_3)$	1100			1025	1048	1083	1083	1140
ν(CO)	1034			1056	1034	1062	1057	1084
ρ''_t(OH)	270			311	379	264	545	—
ν(OH)-silanol				3710	3340	3528	3467	3454, 3717
δ(COSi)				—	—	—	—	351
$\rho''_t(CH_3)$				—	—	—	118	120

Note. Columns are identified by the figure number in this report.

[a] Taken from Refs. (51, 52).

[b] DFT predictions have been scaled by 0.962 to obtain the best match between the theoretical and experimental spectra for gaseous methanol.

[c] These bands are also caused by silica hydroxyl groups.

and ethanol adsorbed on silica, and these spectra were subtracted from each other to produce the difference-spectra in Fig. 2b. The bands observed in these spectra are summarized in Table 2 and compared with DFT predictions from this work for adsorbed ethanol (discussed in the next section) and literature data for gaseous ethanol. The spectrum in Fig. 2b(i) was collected at an ethanol pressure of 2 Pa, which corresponds to a surface coverage of ~40 μmol/g. In general, $\nu_s(CH_3)$ and $\nu_{as}(CH_3)$ modes of vibration are shifted to lower wavenumbers by 11 and 17 cm^{-1}, respectively, whereas the perturbation of O–H stretching modes is more evident, with a shift to lower wavenumbers of 350 cm^{-1} relative to gaseous ethanol. The band at 3740 cm^{-1} appears to be caused by weakly adsorbed ethanol, since it is not present after evacuation of the sample at room temperature (Fig. 2b(ii)). Moreover, shifts in opposite directions of less than 20 cm^{-1} are observed for both $\nu(CH_2)$ and $\delta(CH_2)$ modes, suggesting the presence of different types of adsorbed ethanol.

The sample was outgassed overnight in vacuum and infrared absorption spectra were collected. The corresponding difference-spectrum is included in Fig. 2b(ii), from which it can be seen that some ethanol (~20 μmol/g) remains on the surface after evacuation at room temperature. Among the bands observed in this case, which are summarized in Table 2, two new bands are observed at 2958 and 2856 cm^{-1}. The former band can be assigned to $\nu(CH_2)$, but assignment of the latter band is less certain, being caused perhaps by overtones or combinations of methyl and/or methylene deformation modes in view of the fact that C–H stretches in ethanol occur typically above 2900 cm^{-1}. The sample was subsequently outgassed for 2 h at 473 K and infrared absorption spectra collected. The corresponding difference-spectrum is included in Fig. 2b(iii), and it shows that some ethanol remains on the surface as evidenced by a weak ν(OH) band near 3450 cm^{-1}. The sample was then outgassed at 573 K for 2 h. The corresponding difference-spectrum is included in Fig. 2b(iv), and the band positions are summarized in Table 2. On the basis of this spectrum, we conclude that most of ethanol adsorbs molecularly on silica at room temperature, and essentially all molecularly adsorbed ethanol can be removed by evacuation at 573 K. A small amount (~5 μmol/g) of strongly adsorbed species, most likely ethoxy fragments, remains on the surface, as evidenced by the bands in the 2800–3000 cm^{-1} region of Fig. 2b(iv).

2,2,2-Trifluoroethanol adsorption. Infrared absorption spectra were collected at room temperature for silica, gaseous tfetoh, and tfetoh adsorbed on silica, and these spectra were subtracted from each other to produce the difference-spectra in Fig. 2c. The bands observed in these

TABLE 2

Wavenumbers (cm^{-1}) for the Fundamental Modes of Vibration of Ethanol in the Gas Phase and Adsorbed on Silica at Room Temperature

	Experimental				DFT prediction[b]				
Description	Gas[a]	Adsorbed 2b(i)	Adsorbed 2b(ii)	Adsorbed 2b(iv)	Gas (C_s)	Gas (C_1)	Adsorbed 5(a)	Adsorbed 5(b)	Ethoxy 11(a)
ν(OH)	3676	3326, 3740[c]	3400[c]		3667	3655	3650	3710	—
$\nu''_{as}(CH_3)$	(2989)	(2982)	(2982)	(2982)	3040	3034	3042	3034	3152
$\nu'_{as}(CH_3)$	(2989)	(2982)	(2982)	(2982)	3034	3020	3032	3028	3142
$\nu''(CH_2)$	2948		2958	2958	2932	3001	3012	2955	3048
$\nu_s(CH_3)$	2943	2932	2928	2930	2959	2943	2949	2913	3066
$\nu'(CH_2)$	2900	2908, 2880	2874	2908, 2874	2902	2913	2946	2888	3012
			2856	2856					
$\delta'(CH_2)$	1490	1496, 1484	1706		1489	1479	1480	1490	1535
$\delta'_{as}(CH_3)$	(1452)	(1452)	(1456)		1466	1459	1460	1466	1516
$\delta''_{as}(CH_3)$	(1452)	(1452)	(1456)		1449	1455	1457	1449	1502
$\rho'_r(CH_2)$	1415	1400	1400		1413	1385	1391	1426	1440
$\delta'_s(CH_3)$	1394	1378			1364	1363	1368	1365	1409
$\rho''_t(CH_2)$	1251				1261	1329	1241	1260	1321
δ'(COH)	1241				1231	1239	1327	1284	—
ν_{as}(CCO)	1089				1085	1060	1058	1101	—
$\rho''_r(CH_3)$	1062				1144	1106	1103	1145	1183
$\rho'_r(CH_3)$	1033				1013	1029	1042	1037	1126
ν_s(CCO)	885				883	868	872	886	—
$\rho''_r(CH_2)$	801				795	778	785	792	819
δ(CCO)	419				403	407	432	419	373
$\rho''_t(CH_3)$	243				239	257	257	241	265
ρ''_t(OH)	201				295	281	359	249	—
ν(OH)-silanol	—				3722	—	3399	3541	—
ν(CO)	—				—	—	—	—	1152
ν(CC)	—				—	—	—	—	976
δ(COSi)	—				—	—	—	—	166

Note. The degeneracy of the bands listed in parenthesis has not been resolved, or, in the case of adsorbed ethanol, may be lost. Columns are identified by the figure number in this report.

[a] Taken from Ref. (59).

[b] DFT predictions have been scaled by 0.965 to obtain the best match between the theoretical and experimental spectra for gaseous ethanol.

[c] These bands may also be due to absorption by perturbed silica hydroxyls.

spectra are summarized in Table 3 and compared with DFT predictions from this work for adsorbed tfetoh (discussed in the next section) and literature data for gaseous tfetoh. The spectrum in Fig. 2c(i) was collected at a tfetoh pressure of 2 Pa, which corresponds to a surface coverage of ~130 μmol/g. The C–H stretching and bending modes of vibration are affected slightly, while the perturbation of the O–H stretching mode is more evident. Fundamental vibrations of the CF_3 group are not observed due to the opacity of the sample. In particular, $\nu_{as}(CH_2)$, $\nu_s(CH_2)$, $\delta(CH_2)$, and $\rho_w(CH_2)$ are shifted by −2, 11, −2, and 6 cm^{-1}. The $\delta(CH_2)$ overtone at 2892 cm^{-1} and ν(OH) are shifted to lower wavenumbers by 4 and 279 cm^{-1}, respectively, relative to gaseous tfetoh. The fact that $\nu_{as}(CH_2)$ and $\delta(CH_2)$ shift in a direction opposite to $\nu_s(CH_2)$ suggests the presence of a mixture of modes of tfetoh adsorption.

The sample was outgassed overnight in vacuum and infrared absorption spectra were collected. The corresponding difference-spectrum is included in Fig. 2c(ii), from which it can be seen that some tfetoh (~40 μmol/g) remains on the surface after evacuation at room temperature. In addition, two ν(OH) bands at 3686 and 3418 cm^{-1} are observed, suggesting the presence of at least two types of adsorbed tfetoh. This interpretation is supported by the disappearance of the band at 2892 cm^{-1} and the appearance of two bands at 2927 and 2856 cm^{-1} for the $\delta(CH_2)$ overtone. The sample was subsequently outgassed at 473 K for 2 h and infrared absorption spectra collected. The corresponding difference-spectrum is included in Fig. 2c(iii), from which we conclude that all adsorbed tfetoh can be removed by evacuation at 473 K. These findings are in agreement with previous studies of tfetoh adsorption on silica at room temperature where the formation of 2,2,2-trifluoroethoxy species was not observed on a sample pretreated at 673 K, whereas the ethoxylation of silica was observed to occur (53).

TABLE 3

Wavenumbers (cm^{-1}) for the Fundamental Modes of Vibration of 2,2,2-Trifluoroethanol in the Gas Phase (C_s Point Group) and Adsorbed on Silica at Room Temperature

	Experimental			DFT prediction[b]			
Description	Gas[a]	Adsorbed 2c(i)	Adsorbed 2c(ii)	Gas	Adsorbed 5(c)	Adsorbed 5(d)	Tfetxy 11(c)
ν(OH)	3657	3378[c]	3686, 3418[c]	3662	3627	3431	—
$\nu''_{as}(CH_2)$	2992	2990	2986	2969	3048	3012	3004
$\nu'_{s}(CH_2)$	2949	2960	2960	2923	2963	2929	2929
$2\delta(CH_2)$	2896	2892	2927, 2856				
$\delta(CH_2)$	1458	1456	1462	1459	1444	1437	1447
$\rho'_{w}(CH_2)$	1414	1420	1422	1438	1396	1379	1387
δ'(OH)	1367	1370		1194	1225	1414	—
$\nu''_{as}(CF_3)$	1292			1147	1149	1136	1142
$\nu'_{as}(CF_3)$	1263			1108	1111	1120	1136
$\nu_{s}(CF_3)$	1180–1190			1253	1253	1230	1255
$\rho''_{t}(CH_2)$	1141			1268	1343	1264	1284
ν(CO)	1088			1092	1071	1104	1163
$\rho''_{r}(CH_2)$	940			949	913	913	944
ν(CC)	830			799	806	791	804
$\delta'_{s}(CF_3)$	668			618	631	633	623
$\delta'_{as}(CF_3)$	548			521	517	513	509
$\delta''_{as}(CF_3)$	539			505	504	500	501
δ(CCO)	416			398	410	397	381
$\rho''_{r}(CF_3)$	364			338	321	336	343
$\rho'_{r}(CF_3)$	282			218	244	232	219
ρ''_{t}(OH)	238			137	380	710	—
$\rho''_{t}(CF_3)$	120			93	115	202	65
ν(OH)-silanol	—	—	—	3857	3630	3825	—
δ(COSi)	—	—	—	—	—	—	213

Note. Columns are identified by the figure number in this report.

[a] Taken from Refs. (60, 61).

[b] The best match between the theoretical and experimental spectra for gaseous 2,2,2-trifluoroethanol was obtained with a scaling factor of 1.00.

[c] These bands may also be due to absorption by perturbed silica hydroxyls.

DFT Calculations

Molecular adsorption. To study the adsorption and reaction of methanol, ethanol, and tfetoh on silica, various clusters were considered that involve alcohol or alkoxy fragments interacting with silica hydroxyls and siloxane bridges. These clusters represent (1) molecular adsorption of the alcohol involving a single hydrogen bond with a silanol group, (2) molecular adsorption of the alcohol involving two and three hydrogen bonds with either vicinal silica hydroxyls or a silanol group contiguous to a siloxane bridge, (3) adsorbed alkoxy species, and (4) transition states for the alkoxylation of silica hydroxyls and siloxane bridges.

Alcohols can interact with a silanol group via donation of electron density from the oxygen atom in the alcohol to the silanol group or via donation of electron density from the oxygen atom in the silanol group to the alcohol. These modes of adsorption correspond to the alcohol acting as a base or an acid, respectively. Optimized structures for hydrogen-terminated clusters, and hydroxyl-terminated clusters in those cases involving methanol, that represent these two modes of alcohol adsorption are included in Figs. 4 and 5. Structural parameters for the hydrogen-terminated clusters were determined from full optimizations, whereas those parameters for hydroxyl-terminated clusters were obtained from partial optimizations in which the Si–O and O–H bond lengths as well as the SiOH angles for the three terminating hydroxyl groups were kept constant at values of 165 pm, 98 pm, and 121.4°, respectively, which resulted from a full optimization of $Si(OH)_4$. Predicted energetics for the corresponding adsorption and reaction processes are included in Tables 4–6. The strength of hydrogen bonds between methanol, ethanol, and tfetoh and a single silanol group is predicted to be 26–38 kJ/mol for the alcohols acting as bases and 15–34 kJ/mol for the alcohols acting as acids. These results are in agreement with the previously cited value of 22–28 kJ/mol expected for these types of hydrogen bonds. It appears that, except for tfetoh, the mode of adsorption in which the alcohol behaves as a base, or hydrogen-bond acceptor (Figs. 4a, 5a, and 5c) is slightly more favorable, which is in agreement with previous quantum-chemical (7) and spectroscopic (27, 53, 54) studies

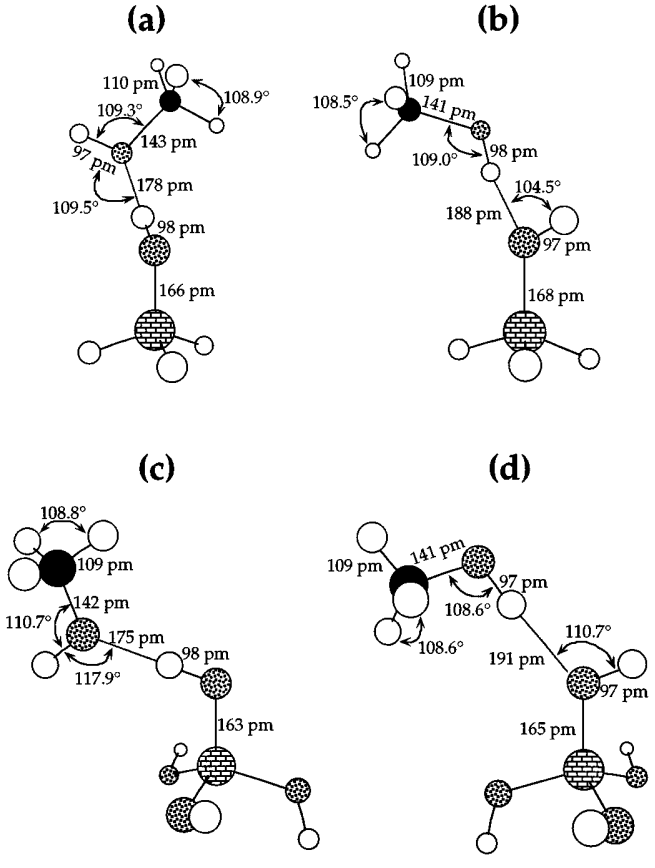

FIG. 4. Structural models for the molecular adsorption of methanol on hydrogen-terminated (a and b) and hydroxyl-terminated (c and d) silanol groups, with the alcohol behaving as a base or hydrogen-bond acceptor (a and c) and behaving as an acid or hydrogen-bond donor (b and d). The hydroxyl-terminated clusters were determined from partial optimizations in which the Si–O and O–H bonds lengths as well as the SiOH angles for the three terminating hydroxyls were kept constant at the values of 165 pm, 98 pm, and 121.4°, respectively, obtained from an optimization of $Si(OH)_4$. The terminating hydroxyls in clusters (c and d) were modelled using the basis set 3-21+G* while the basis set 6-31+G* was used for the remainder of each cluster.

of alcohol adsorption on silica. The additional stability of acidic tfetoh versus basic tfetoh on a silanol group is caused in our models by additional hydrogen-bonding interactions between the CF_3 group and the silanol group. It can be seen in Table 4 that hydrogen-bonding energies are slightly underestimated when using hydrogen-terminated instead of hydroxyl-terminated clusters; however, the trends are predicted to be the same in both cases. In any case, the energetic differences between the alcohols playing the role of bases versus the role of acids are within the error of our calculations, given the known shortcomings of DFT methods in describing hydrogen-bonding and van der Waals complexes, and in view of the dependence of the basicity of oxygen on cluster termination (55–57).

According to the results in Tables 1–3, when the alcohol acts as a base, ν(OH) is shifted to lower wavenumbers by 1–35 cm^{-1} for the alcohol hydroxyl and by ~323 cm^{-1} for the silica hydroxyl, where the predicted wavenumber (scaled by 0.962) for a free silanol group is 3710 cm^{-1}. In addition, bands corresponding to symmetric and antisymmetric stretches of C–H bonds in methyl and methylene groups are predicted to shift to higher wavenumbers by 10–80 cm^{-1} relative to gas-phase spectra, while C–O stretches are predicted to shift to lower wavenumbers by 21–27 cm^{-1}. These predictions are in agreement with empirical evidence, suggesting that a decrease in the electron density of the alkyl group leads to an increase in the C–H stretching frequency, and vice versa (58). When the alcohol acts as an acid, ν(OH) is shifted to higher wavenumbers by 31–55 cm^{-1} for methanol and ethanol, whereas for tfetoh this band is shifted to lower wavenumbers by 231 cm^{-1}. The ν(OH) band for the silanol group for this acidic mode of alcohol adsorption is predicted to shift to lower wavenumbers by ~182 cm^{-1} in the case of methanol and ethanol, and by 30 cm^{-1} in the case of tfetoh. Moreover, symmetric and antisymmetric stretches of C–H bonds in methyl and methylene groups are shifted to lower wavenumbers by 16–22 cm^{-1}, while wavenumbers for C–O stretches increase

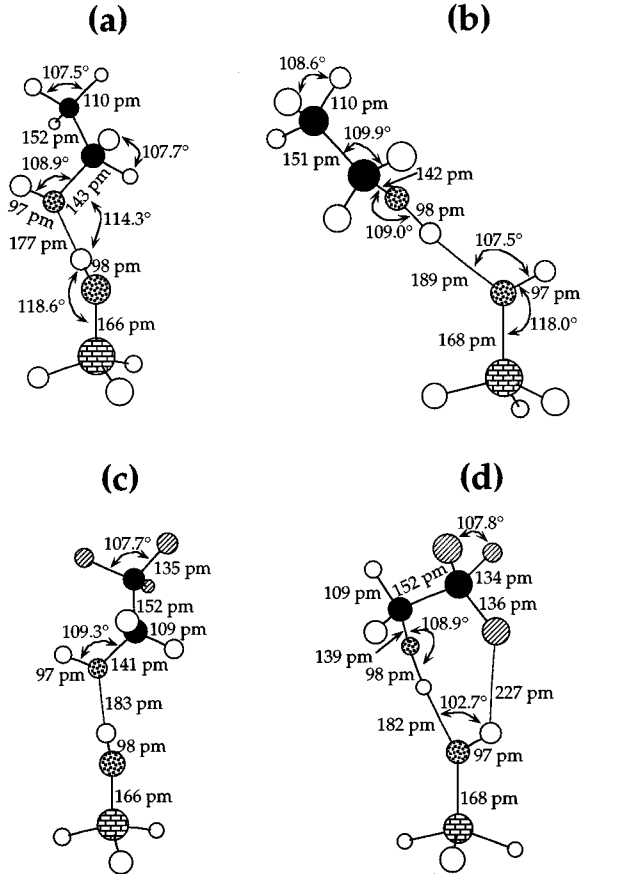

FIG. 5. Structural models for the molecular adsorption on hydrogen-terminated silanol groups of ethanol behaving as (a) a base and (b) an acid, and of 2,2,2-trifluoroethanol behaving as (c) a base and (d) an acid.

TABLE 4

Energetics (kJ/mol) Predicted for the Adsorption and Reaction of Methanol on Silica

R × n at 298 K	ΔE[a]	ΔH	ΔG
Adsorption and reaction			
$MeOH + HOSiH_3 \rightarrow$ 4(a): $MeOH(base) \leftarrow HOSiH_3$	−33	−26	7
$MeOH + HOSiH_3 \rightarrow$ 4(b): $MeOH(acid) \rightarrow HOSiH_3$	−23	−16	16
$MeOH + Si(OH)_4 \rightarrow$ 4(c): $MeOH(base) \leftarrow HOSi(OH)_3$	−38	—	—
$MeOH + Si(OH)_4 \rightarrow$ 4(d): $MeOH(acid) \rightarrow HOSi(OH)_3$	−25	—	—
$MeOH + Si(OH)_4 \rightarrow$ 6(b): $MeOH \leftrightarrow (HO)_2Si(OH)_2$	−46	−35	−38
$MeOH + HOSiH_3 \rightarrow$ 7(b): $H_2O\cdots MeO{-}SiH_3$	−26	−19	14
$7(b) \rightarrow H_2O + 7(a)$: $MeO{-}SiH_3$	24	17	−14
$MeOH + H_3SiOSi(OH)H_2 \rightarrow 6(a)$	−32	−27	18
$6(a) \rightarrow 7(c)$: $H_3SiOH\cdots MeOSi(OH)H_2$	26	25	15
$MeOH +$ 3-silanols $\rightarrow 6(c)$	−91	—	—
Transition states			
$4(a) \rightarrow$ TS1	317	304	315
$4(b) \rightarrow$ TS2	107	96	115
$6(a) \rightarrow$ TS3	129	119	121
$6(b) \rightarrow$ TS4	322	309	309
$6(b) \rightarrow$ TS5	128	117	117
Proton removal			
$MeOH \rightarrow MeO^- + H^+$	1618	1575	1577
$Me_3COH \rightarrow Me_3CO^- + H^+$	1593	1552	1554

Note. Species are identified by their figure number in this report.
[a] These values are not corrected by changes in the zero-point energies.

TABLE 5

Energetics (kJ/mol) Predicted for the Adsorption and Reaction of Ethanol on Silica

R × n at 298 K	ΔE[a]	ΔH	ΔG
Adsorption and reaction			
$EtOH + HOSiH_3 \rightarrow$ 5(a): $EtOH(base) \leftarrow HOSiH_3$	−34	−26	4
$EtOH + HOSiH_3 \rightarrow$ 5(b): $EtOH(acid) \rightarrow HOSiH_3$	−22	−15	14
$EtOH + HOSiH_3 \rightarrow$ 11(b): $H_2O\cdots EtO{-}SiH_3$	−26	−20	15
$11(b) \rightarrow H_2O +$ 11(a): $EtO{-}SiH_3$	23	16	−16
Transition States			
$5(a) \rightarrow$ TS6	300	285	297
$5(b) \rightarrow$ TS7	107	96	117
Proton Removal			
$EtOH \rightarrow EtO^- + H^+$	1605	1562	1565

Note. Species are identified by their figure number in this report.
[a] These values are not corrected by changes in the zero-point energies.

by 3–12 cm^{-1}. These observations in combination with the FTIR data presented previously, where various bands for C–H stretching and deformation modes shifted in opposite directions, suggest the presence of both the basic and acidic modes of alcohol adsorption on silica.

At low surface coverages, more than one hydrogen bond is expected to form between the alcohol and hydroxyl groups and/or siloxane bridges on the surface of silica (5–7, 18, 19). To study this situation, clusters comprised of methanol interacting with (1) a silanol group and a contiguous siloxane bridge and (2) geminal silanols were optimized, resulting in the structures in Figs. 6a and 6b. In both cases, a distorted ring is formed in which electron density is donated from a silanol group to the alcohol and from the alcohol to the SiO–Si bridge or the other silanol, respectively. The energy of interaction predicted for the formation of the two hydrogen bonds present in the clusters is 32–46 kJ/mol, as shown in Table 4. Similar results were obtained for the adsorption of ethanol and tfetoh.

Calculations were performed for the adsorption of the alcohols on a surface site that allows for the formation of three hydrogen bonds between the adsorbed alcohol and the site. The optimized structure for the case of methanol adsorption is included in Fig. 6c. The predicted heats for this mode of adsorption for methanol, ethanol, and tfetoh are 91, 85, and 85 kJ/mol, respectively. Assuming the clusters to be feasible, these values would be in agreement with our microcalorimetric data and with the expected strength of 22–28 kJ/mol per hydrogen bond. However, a more detailed study of this possibility of forming bifurcated hydrogen bonds between alcohols and silanol groups, as depicted

TABLE 6

Energetics (kJ/mol) Predicted for the Adsorption and Reaction of 2,2,2-Trifluoroethanol on silica

R × at 298 K	ΔE[a]	ΔH	ΔG
Adsorption and reaction			
$TFEtOH + HOSiH_3 \rightarrow$ 5(c): $TFEtOH(base) \leftarrow HOSiH_3$	−35	−27	−92
$TFEtOH + HOSiH_3 \rightarrow$ 5(d): $TFEtOH(acid) \rightarrow HOSiH_3$	−42	−34	−95
$TFEtOH + HOSiH_3 \rightarrow$ 11(d): $H_2O\cdots TFEtO{-}SiH_3$	−25	−18	−80
$11(d) \rightarrow H_2O +$ 11(c): $TFEtO{-}SiH_3$	21	14	−18
Transition States			
$5(c) \rightarrow$ TS8	334	321	338
$5(d) \rightarrow$ TS9	129	117	128
Proton Removal			
$TFEtOH \rightarrow TFEtO^- + H^+$	1517	1476	1382

Note. Species are identified by their figure number in this report.
[a] These values are not corrected by changes in the zero-point energies.

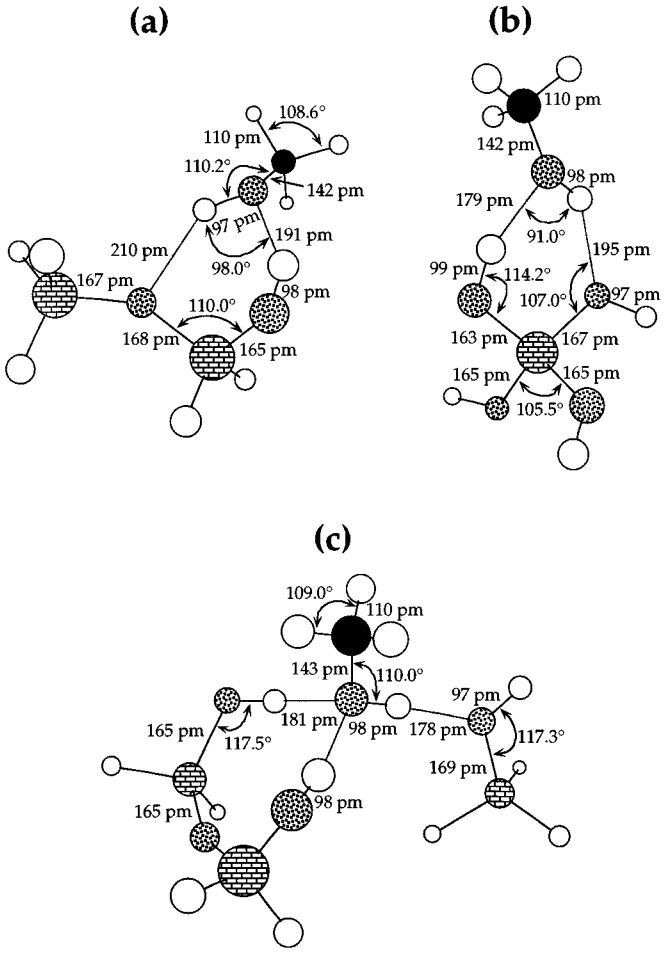

FIG. 6. Structural models for the molecular adsorption of methanol (a) on a silanol group contiguous to a siloxane bridge via two hydrogen bonds, (b) on geminal silanol groups, and (c) on a site allowing for the formation of three hydrogen bonds. The two terminal hydroxyls of the geminal silanols were modelled using the basis set 3-21+G* while the basis set 6-31+G* was used remainder of the cluster, and for all the other clusters.

in Fig. 6c, is required given that higher-level *ab initio* calculations support the formation of relatively linear hydrogen bonds in water clusters. Thus, the high energies of alcohol adsorption measured at low coverages can be interpreted in terms of ring-like structures like those in Figs. 6a and 6b, where the alcohol acts both as a hydrogen-bond donor and acceptor, with perhaps weak hydrogen bonding with next-neighbor silanol groups. This scenario would correspond to the cluster in Fig. 6c, but with methanol tilted so that three of the four hydroxyl groups involved in hydrogen bonding, including that of methanol, become nearly coplanar. In addition, the formation of ring-like structures upon interaction of neighboring alcohol molecules can be proposed, which aggregate into polymeric chains bound by three hydrogen bonds per monomer, as depicted in models obtained from previous quantum-chemical calculations (5–7).

Formation of methoxy species. Energetics for the formation of methoxy species upon reaction of methanol with silanol groups and siloxane bridges are included in Table 4, with the corresponding optimized clusters shown in Fig. 7. Infrared absorption bands for the structure in Fig. 7c are included in Table 1. As mentioned previously, methoxy species can form on silica via protonation of methanol by a silanol group or via protonation and subsequent cleavage of Si–OH bonds or SiO–Si bridges by methanol. Optimized structures for the transition states corresponding to the hydrogen-terminated clusters of methoxy species in Fig. 7 are shown in Fig. 8. The transition state for the protonation of methanol by a hydrogen-terminated silanol group is hereafter named TS1. The transition states corresponding to the protonation and subsequent cleavage of Si–OH bonds or SiO–Si bridges are identified in Fig. 8 as TS2 and TS3, respectively. It was verified that TS1, TS2, and TS3 are first-order saddle points by ensuring that they have only one imaginary (negative) vibrational frequency. Furthermore, to verify that these transition states are, in fact, the first-order saddle points connecting the desired reactants and products, IRC calculations were performed for TS1 and TS2, the results of which are included in

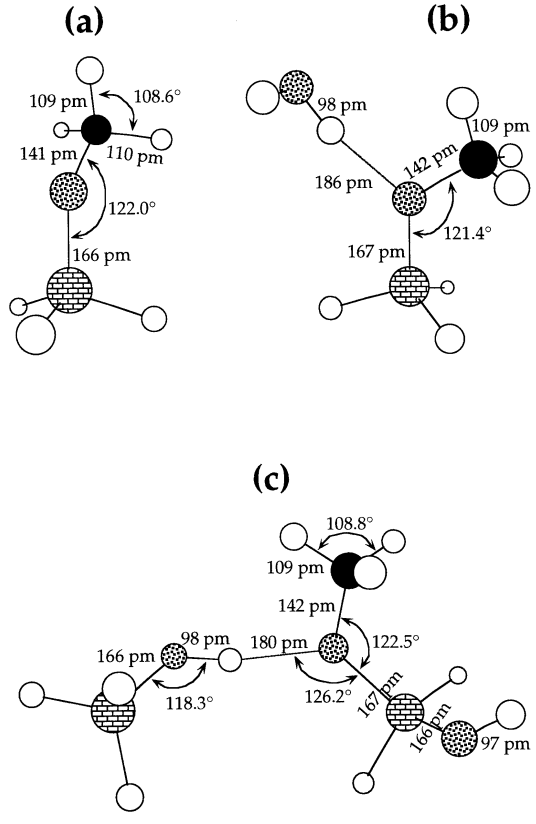

FIG. 7. Structural models for methoxy species (a) isolated, (b) hydrogen-bonded to water (resulting from the esterification of a silanol group), and (c) hydrogen-bonded to a neighboring silanol group produced by the cleavage of a siloxane bridge.

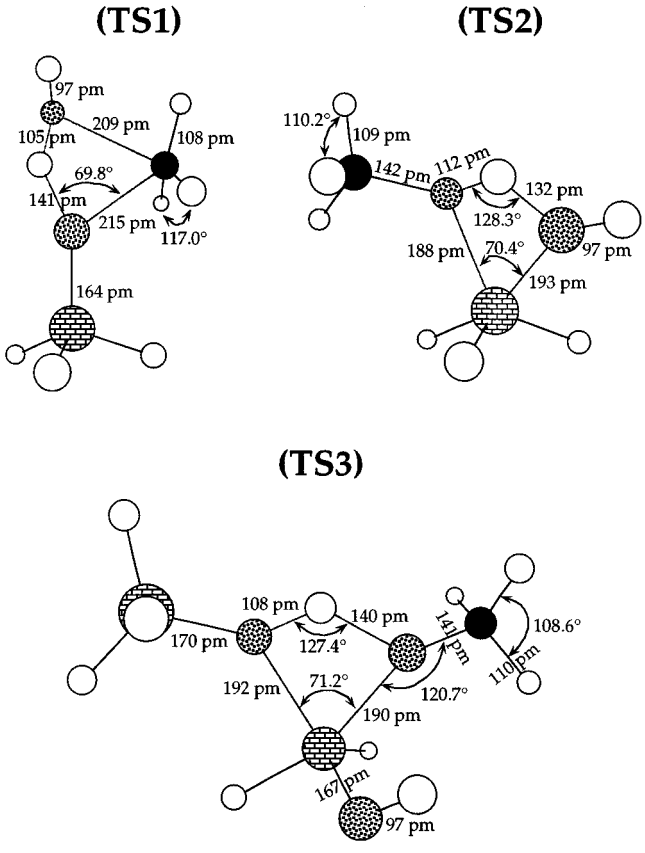

FIG. 8. Structural models for transition states involved in the formation of methoxy species via protonation of methanol by a hydrogen-terminated silanol group (TS1), protonation and subsequent cleavage of a hydrogen-terminated silanol group by the alcohol (TS2), and protonation and subsequent cleavage of a siloxane bridge by the alcohol (TS3).

Fig. 9. The structural models included in Figs. 9a and 9b correspond to the last point on each side of the IRC curves, and they verify in both cases that the desired reaction products are obtained. The validity of TS3 was verified by ensuring that the mode of vibration corresponding to the negative vibrational frequency is analogous to that of TS2.

In contrast to the corresponding structures of adsorbed methanol (Fig. 4a) and methoxy species (Fig. 7b), TS1 shows rehybridization of the carbon atom from sp^3 to a nearly sp^2 state after removal of the hydroxyl group. In addition, the O–H bond in the silanol group is stretched by 44 pm. This transition state resembles a distorted alkoxonium ion. The activation energy for the formation of methoxy species through this pathway is shown in Table 4 to be 304 kJ/mol, which is higher than the upper limit of 220 kJ/mol that can be inferred from the treatments used in previous studies of the methoxylation of silica (10, 17–19). This difference suggests that methoxy species may form predominantly by reaction of adsorbed methanol with siloxane bridges or by an alternate pathway.

The predicted low rate of methoxylation of silica via TS1 can be interpreted in terms of the charge localized in the methyl group of the transition state. The Mulliken charges of the methyl group in adsorbed methanol (Fig. 4a) and methoxy species (Fig. 7b) on silica are estimated to be 0.23*e* and 0.17*e*, respectively. However, the charge of the methyl group in the transition state is 0.38*e*. The activation process thus requires partial separation of charge, which is made difficult by the weak acidity of silica and the instability of $CH_3^{\delta+}$, methyl carbenium ions. In this respect, protonation of higher alcohols by silanol groups to form alkoxy species should be more favorable via transition states analogous to TS1, since they would involve more stable carbenium ions. Moreover, the rate of reaction via this pathway is expected to be higher on the surface of more acidic oxides like alumina or zeolites.

The formation of methoxy species via protonation of a silanol group by adsorbed methanol (Fig. 4b) is modelled by TS2. In this case, the O–H bond in methanol is stretched by 14 pm. The activation energy for the formation of methoxy species through this pathway is shown in Table 4 to be 96 kJ/mol. The lower activation energy predicted for this mechanism suggests that methoxy species may form preferentially via TS2 instead of TS1; that is, methanol behaves as an acid when forming methoxy species via interactions with silanol groups. This behavior is also observed upon adsorption and reaction of methanol with siloxane bridges (Fig. 6a) to form methoxy species, as depicted by TS3. In this case, the activation energy is predicted to be 119 kJ/mol, again suggesting that methoxy species may form preferentially via TS3 instead of TS1. Previous studies (11) of the methoxylation of silica via the esterification of silanols and the opening of siloxane bridges at temperatures between 423 and 463 K have found that the Gibbs free-energy of activation of the former pathway is only 4 kJ/mol higher than for the latter pathway. This result suggests that the activation energy is underestimated from the hydrogen-terminated clusters in Figs. 4a and 8 (TS1), most likely because of the poor description of the basicity of oxygen atoms in hydrogen-terminated clusters (55–57). In either case, our computations predict that the activation energy is too high for the methoxylation of silica at room temperature, which is in agreement with our FTIR data.

The rate of methoxylation of silica via protonation of silanol groups or siloxane bridges is controlled mainly by the acid strength of methanol and the extent of delocalization of electron density in the four-member ring present in transition states TS2 and TS3. The partial removal of a proton from methanol in TS2 can be observed by comparing the charges of 0.46*e*, 0.55*e*, and 0.58*e* for this hydrogen atom in gaseous methanol, adsorbed methanol (Fig. 4b), and TS2, respectively. In this regard, the rate of alkoxylation of silica via TS2, TS3, and their analogs should not be very sensitive to the type of alcohol considered since, as shown in

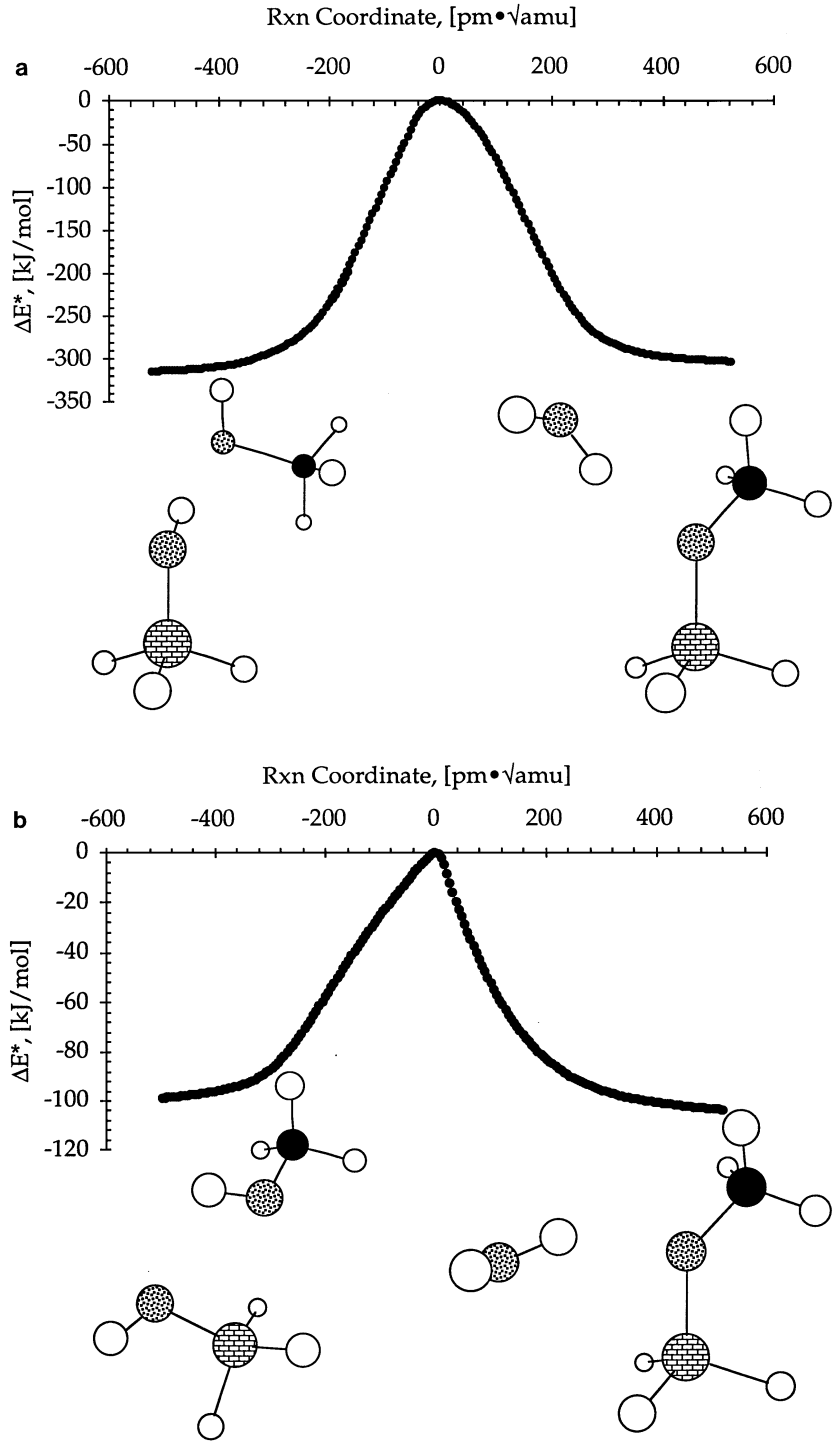

FIG. 9. IRC curves for verification of transition states (a) TS1 and (b) TS2. Energies are defined relative to that of the corresponding transition state. The structural models correspond to the last point on each side of the IRC curves.

Tables 4 and 5, the removal of a proton from a tertiary alcohol such as tert-butanol is predicted by DFT to be only 10–23 kJ/mol more favorable than from methanol or ethanol. Finally, it should be noted that a configuration similar to the four-member ring in TS2 and TS3 is also present in TS1. However, the greater radial expansion of the p-orbitals in silicon versus those in carbon allows for greater delocalization of electron density in TS2 and TS3 than in TS1, thus contributing to a lower activation barrier. This view is supported by the fact that the carbon atom rehybridizes to a

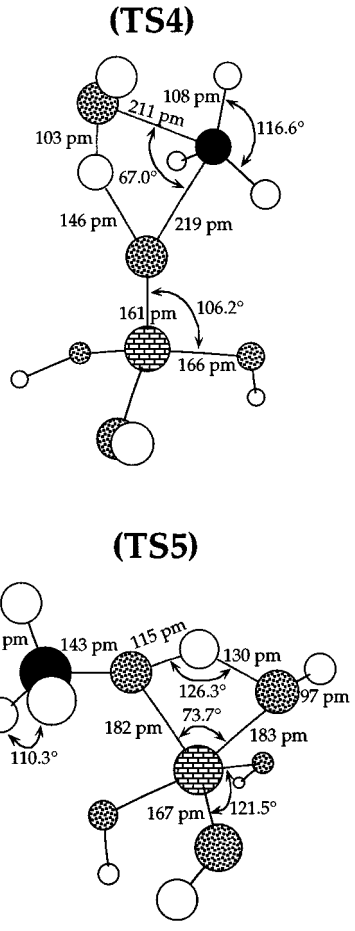

FIG. 10. Structural models for transition states involved in the formation of methoxy species via protonation of methanol by a hydroxyl-terminated silanol group (TS4) and protonation of a hydroxyl-terminated silanol group by the alcohol (TS5). To be consistent with calculations performed for the cluster in Fig. 6(b), two of the termination hydroxyls were modelled using the basis set 3-21+G* while the basis set 6-31+G* was used for the remainder of the cluster.

nearly sp^2 state in TS1, suggesting the presence of an effectively empty p-orbital, whereas silicon does not exhibit this behavior in TS2 or TS3.

To improve the predictions obtained for the activation energy of methoxylation via the protonation of silanol groups, transition states were located as before for the two possible pathways for reaction between methanol and silanol groups, but this time using the hydroxyl-terminated cluster in Fig. 6b. In this ring-like structure, both reaction pathways can potentially occur starting with the same structure. The optimized structures for the transition states are included in Fig. 10, where the clusters corresponding to the protonation of methanol by the silanol group is identified as TS4 and the clusters corresponding to the protonation and subsequent cleavage of the Si–OH bond by the alcohol is identified as TS5. As shown in Table 4, the activation energy barriers are estimated to be 309 and 117 kJ/mol, respectively. These values agree with our conclusion that the esterification of silanol groups appears to occur via the protonation and cleavage of Si–OH bonds by the adsorbed alcohol. The energy barrier calculated for this preferred pathway is nearly equal to that calculated from TS3 for the opening of siloxane bridges. A comparison of the energetics based on TS2 versus TS5, suggests that hydrogen-termination of the clusters leads to an underestimation of the activation barrier by ~21 kJ/mol for the preferred alkoxylation pathway, as opposed to hydroxyl-termination of clusters. This difference of 21 kJ/mol will be used later as an approximation of the error involved in the estimation of activation barriers for the ethoxylation and 2,2,2-trifluoroethoxylation of silanols by using the simpler hydrogen-terminated clusters.

Formation of ethoxy and 2,2,2-trifluoroethoxy species. Energetics for the formation of ethoxy and 2,2,2-trifluoroethoxy species (hereafter named tfetxy) are included in Tables 5 and 6, respectively. The clusters used to model the formation of these alkoxy species are shown in Fig. 11, with infrared absorption spectra shown in Tables 2 and 3.

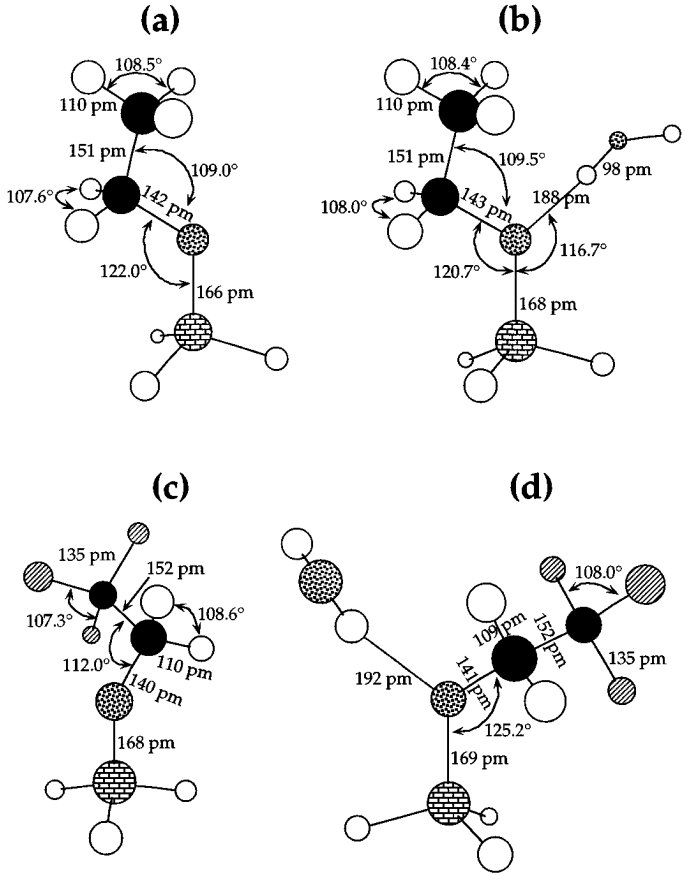

FIG. 11. Structural models for ethoxy species (a) isolated and (b) hydrogen-bonded to water, and for 2,2,2-trifluoroethoxy species (c) isolated and (d) hydrogen-bonded to water.

As in the formation of methoxy species on silica, the formation ethoxy and tfetxy species appears to be favorable energetically. Transition states for the transformation of molecularly adsorbed ethanol and tfetoh were located on the PES, and optimized structures for the transition states of interest are shown in Fig. 12. The transition states for the protonation of ethanol and tfetoh by the silanol group are hereafter named TS6 and TS8, respectively, while those for the protonation of the silanol group by the adsorbed alcohol (or siloxane bridges, with water simulating a produced silanol group) are named TS7 and TS9. It was verified that the transition states TS(6–9) are first-order saddle points by ensuring that they have only one imaginary (negative) vibrational frequency. Furthermore, IRC calculations were performed to verify that these transition states are the first-order saddle points connecting the desired reactants and products. Results of these IRC calculations for TS6 and TS7 are included in Fig. 13. The structural models included in Figs. 13a and 13b correspond to the last point on each side of the IRC curves, and they verify in both cases that the desired reaction products are obtained.

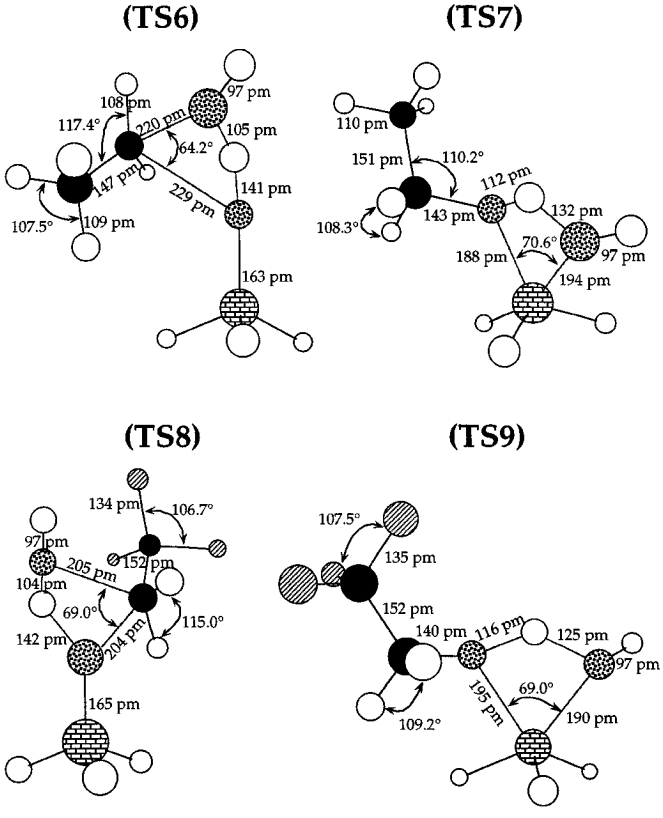

FIG. 12. Structural models for transition states involved in the formation of ethoxy and 2,2,2-trifluoroethoxy species via protonation of the corresponding alcohol by a hydrogen-terminated silanol group (TS6 and TS8, respectively) and via protonation and subsequent cleavage of a hydrogen-terminated silanol group by the corresponding alcohol (TS7 and TS9, respectively).

Results from IRC calculations for TS8 and TS9 are not included in this report, but they are analogous to those for TS6 and TS7.

Transition states TS6 and TS8 show rehybridization of the carbon atom previously bonded to oxygen from sp^3 to a nearly sp^2 state after removal of the hydroxyl group. As in the case of methoxy formation discussed previously, these transition states resemble distorted alkoxonium ions. The activation energies for the formation of ethoxy and tfetxy species through these transition states are shown in Tables 5 and 6 to be 285 and 321 kJ/mol, respectively. These high values result from the required partial separation of charge which is made difficult by the weak acidity of silica and the instability of the ethyl and 2,2,2-trifluoroethyl carbenium ions involved in the activation process. It should be noticed that the ethoxylation of silanol groups is predicted to occur faster than the corresponding methoxylation since ethyl carbenium ions are more stable than their methyl counterparts. On the other hand, inductive effects from electron-withdrawing CF_3 groups make the 2,2,2-trifluoroethyl carbenium ion present in transition state TS8 less stable than its nonfluorinated counterpart in TS6, thus contributing to the higher energy barrier. The activation barrier predicted for ethoxy formation on silica is much higher than the value of 130 kJ/mol estimated previously from kinetic measurements of the dehydrogenation of ethanol to acetaldehyde over highly dehydrated silica (22), which suggests the occurrence of this process via an alternate pathway.

The formation of ethoxy and tfetxy species via protonation of a silanol group (or a siloxane bridge, with water simulating a produced silanol group) by adsorbed ethanol (Fig. 5b) and tfetoh (Fig. 5d) proceeds via transition states TS7 and TS9, respectively. The activation energies for the formation of ethoxy and tfetxy species through these transition states are shown in Tables 5 and 6 to be 96 and 117 kJ/mol, respectively. However, after considering the error of 21 kJ/mol introduced in our calculations by hydrogen-termination of the clusters, these activation barriers are increased to 117 and 138 kJ/mol, respectively. The lower energy barriers predicted for this reaction pathway suggest that ethoxy and tfetxy species form via TS7 and TS9 and not via TS6 and TS8. In addition, the prediction involving TS7 for the ethoxylation of silica is in agreement with the previously referred value of 130 kJ/mol.

CONCLUSION

Methanol, ethanol, and 2,2,2-trifluoroethanol adsorb molecularly on silica at 300 K via hydrogen bonds, with initial heats of interaction of 78, 100, and 90 (± 2) kJ/mol, respectively. The alcohols seem to be bound to silica by three hydrogen bonds at low coverages and two hydrogen bonds at moderate to high coverages. On the basis of these initial heats of adsorption, average hydrogen-bond

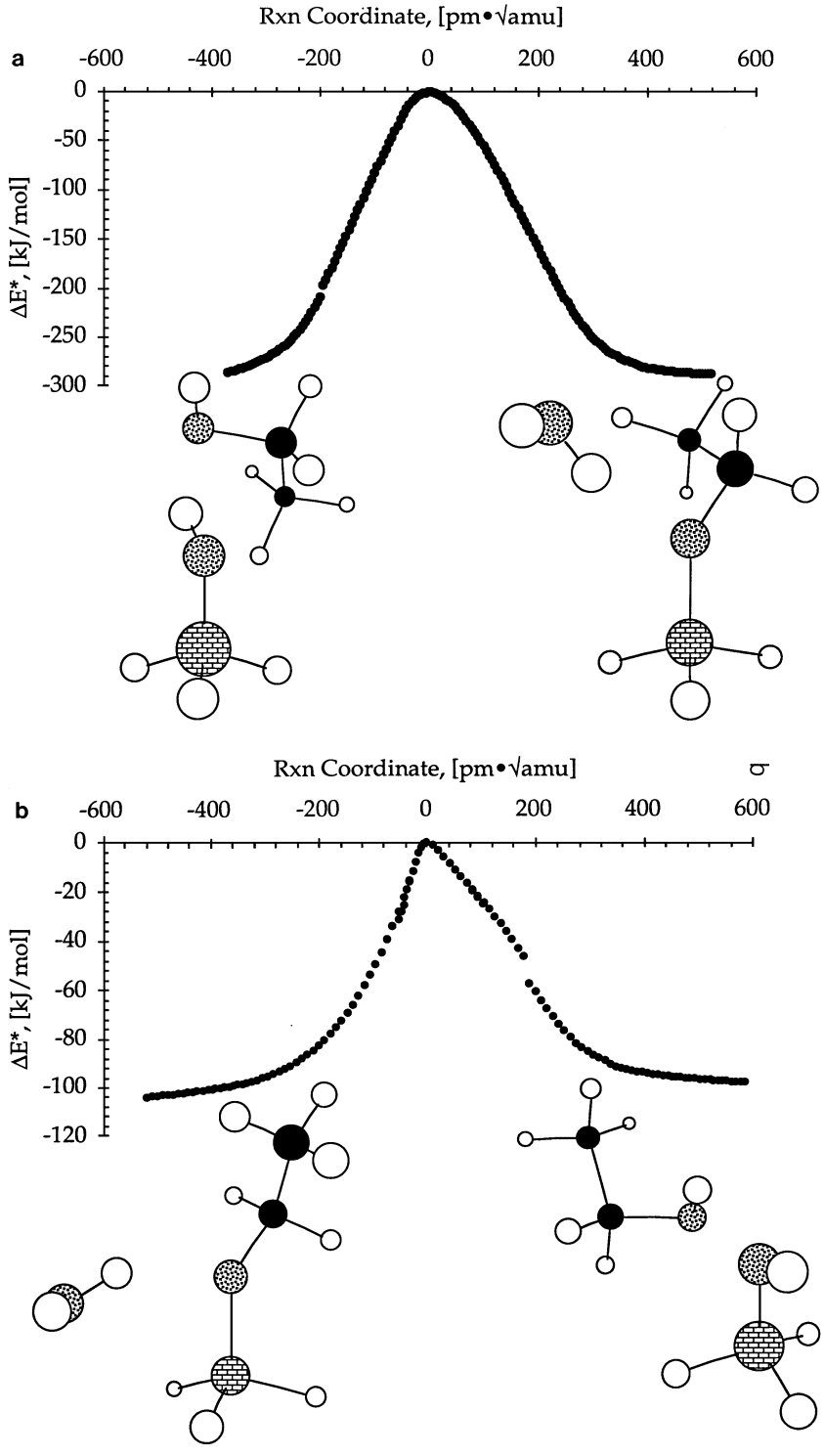

FIG. 13. IRC curves for verification of transition states (a) TS6 and (b) TS7. Energies are defined relative to that of the corresponding transition state. The structural models correspond to the last point on each side of the IRC curves.

strengths of approximately 26, 33, and 30 kJ/mol are obtained for adsorption of methanol, ethanol, and tfetoh, respectively. A slight decrease in the strength of these hydrogen bonds is observed upon fluorination of ethanol due to the inductive effect of CF_3 groups. Adsorbed methanol and 2,2,2-trifluoroethanol can be removed completely from silica by evacuation at 473 K, whereas small amounts of ethoxy species remain on the oxide surface after

evacuation at 573 K. Methanol and ethanol are predicted by DFT calculations to adsorb predominantly as bases, while 2,2,2- trifluoroethanol may prefer to act as an acid.

The alkoxylation of silica can proceed according to two pathways: one pathway involving the protonation of the alcohol by silica hydroxyls and the other involving the protonation and subsequent cleavage of Si–OH bonds or SiO–Si bridges. For the first proposed pathway, the activation energies for the formation of methoxy, ethoxy, and 2,2,2-trifluoroethoxy species on silica are predicted to be within the range 285–321 kJ/mol, whereas for the second pathway these activation barriers are predicted within the range 117–138 kJ/mol. The high activation barrier for the first pathway is caused by the required localization of positive charge in the alkyl group of the transition state, which is made difficult by the weak acidity of silica and the inherent instability of methyl, ethyl, and 2,2,2-trifluoroethyl carbenium ions. The second pathway is controlled mainly by the acid strength of the alcohols and the extent of delocalization of electron density in the four-member ring present in the transition states.

ACKNOWLEDGMENTS

The authors acknowledge the financial support of the Office of Basic Energy Sciences of the Department of Energy and the Center for Clean Industrial and Treatment Technologies, as well as GEM and AOF fellowships awarded to MANS. The authors thank W. S. Millman for providing the IR cell used in our studies.

REFERENCES

1. Wittcoff, H. A., and Reuben, B. G., "Industrial Organic Reactions," J. Wiley, New York, 1996.
2. Seddon, D., *Catal. Today* **15**, 1 (1992).
3. Benaissa, M., Saur, O., and Lavalley, J. C., *Mat. Chem. Phys.* **8**, 387 (1983).
4. Tsutsumi, K., Emori, H., and Takahashi, H., *Bull. Chem. Soc. Japan* **48**(10), 2613 (1975).
5. Pelmenschikov, A. G., Morosi, G., and Gamba, A., *J. Phys. Chem.* **101**, 1178 (1997).
6. Pelmenschikov, A. G., Morosi, G., Gamba, A., Zecchina, A., Bordiga, S., and Paukshtis, E. A., *J. Phys. Chem.* **97**, 11979 (1993).
7. Pelmenschikov, A. G., Morosi, G., and Gamba, A., *J. Phys. Chem.* **96**, 2241 (1992).
8. Shioji, S., Tokami, K., and Yamamoto, H., *Bull. Chem. Soc. Japan* **65**(3), 728 (1992).
9. Morrow, B. A., *J. Phys. Chem.* **81**, 2663 (1977).
10. Morrow, B. A., *J. Chem. Soc.: Faraday Trans. 1* **70**, 1527 (1974).
11. Mertens, G., and Fripiat, J. J., *J. Coll. Interface Sci.* **42**(1), 169 (1973).
12. Takezawa, N., and Kobayashi, H., *J. Catal.* **28**, 335 (1973).
13. Morrow, B. A., Thomson, L. W., and Wetmore, R. W., *J. Catal.* **28**, 332 (1973).
14. Takezawa, N., and Kobayashi, H., *J. Catal.* **25**, 179 (1972).
15. Cruz, M. I., Stone, W. E. E., and Fripiat, J. J., *J. Phys. Chem.* **76**, 3078 (1972).
16. Kiselev, A. V., Lygin, V. I., and Shchepalin, K. L., *Kinet. Catal.* **12**, 154 (1971).
17. Morterra, C., and Low, M. J. D., *J. Phys. Chem.* **73**, 321 (1969).
18. Borello, E., Zecchina, A., Morterra, C., and Ghiotti, G., *J. Phys. Chem.* **71**, 2945 (1967).
19. Borello, E., Zecchina, A., and Morterra, C., *J. Phys. Chem.* **71**, 2938 (1967).
20. Matsumura, Y., Hashimoto, K., and Yoshida, S., *J. Molec. Catal.* **68**, 73 (1991).
21. Matsumura, Y., Hashimoto, K., and Yoshida, S., *J. Catal.* **122**, 352 (1990).
22. Matsumura, Y., Hashimoto, K., and Yoshida, S., *J. Catal.* **117**, 135 (1989).
23. Thamm, H., *J. Chem. Soc.: Faraday Trans. 1* **85**, 1 (1989).
24. Shioji, S., *Kenyu Kiyo: Wakayama Kogyo Koto Senmon Gakko* **23**, 63 (1988).
25. Metcalfe, A., and Shankar, S. U., *J. Chem. Soc.: Faraday Trans. 1* **74**, 1945 (1978).
26. Perfetti, G. A., and Wightman, J. P., *J. Coll. Interface Sci.* **55**(2), 252 (1976).
27. Jeziorowski, H., Knözinger, H., Meye, W., and Müller, H. D., *J. Chem. Soc.: Faraday Trans. 1* **69**, 1744 (1973).
28. Sneh, O., and George, S. M., *J. Phys. Chem.* **99**, 4639 (1995).
29. Bunker, B. C., Haaland, D. M., Ward, K. J., Michalske, T. A., Smith, W. L., Binkley, J. S., Melius, C. F., and Balfe, C. A., *Surf. Sci.* **210**, 406 (1989).
30. Hoffmann, P., and Knözinger, E., *Surf. Sci.* **188**, 181 (1987).
31. Boccuzzi, F., Coluccia, S., Ghiotti, G., Morterra, C., and Zecchina, A., *J. Phys. Chem.* **82**, 1298 (1978).
32. Ferrari, A. M., Garrone, E., Spoto, G., Ugliengo, P., and Zecchina, A., *Surf. Sci.* **323**, 151 (1995).
33. Morrow, B. A., Cody, I. A., and Lee, L. S. M., *J. Phys. Chem.* **80**, 2761 (1976).
34. Morrow, B. A., and Cody, I. A., *J. Phys. Chem.* **80**, 1998 (1976).
35. Morrow, B. A., and Cody, I. A., *J. Phys. Chem.* **80**, 1995 (1976).
36. McDonald, R. S., *J. Phys. Chem.* **62**, 1168 (1958).
37. Cardona-Martínez, N., and Dumesic, J. A., *Adv. Catal.* **38**, 149 (1992).
38. Cardona-Martínez, N., and Dumesic, J. A., *J. Catal.* **125**, 427 (1990).
39. Becke, A. D., *J. Chem. Phys.* **98**, 5648 (1993).
40. Hehre, W. J., Radom, L., and Schleyer, P. v. R., "Ab Initio Molecular Orbital Theory," J. Wiley, New York, 1986.
41. Kohn, W., Becke, A. D., and Parr, R. G., *J. Phys. Chem.* **100**, 12974 (1996).
42. Ziegler, T., *Chem. Rev.* **91**, 651 (1991).
43. Frisch, M. J., Trucks, G. W., Schlegel, H. B., Gill, P. M. W., Johnson, B. G., Robb, M. A., Cheeseman, J. R., Keith, T., Petersson, G. A., Montgomery, J. A., Raghavachari, K., Al-Laham, M. A., Zakrzewski, V. G., Ortiz, J. V., Foresman, J. B., Cioslowski, J., Stefanov, B. B., Nanayakkara, A., Challacombe, M., Peng, C. Y., Ayala, P. Y., Chen, W., Wong, M. W., Andres, J. L., Replogle, E. S., Gomperts, R., Martin, R. L., Fox, D. J., Binkley, J. S., Defrees, D. J., Baker, J., Stewart, J. P., Head-Gordon, M., Gonzalez, C., and Pople, J. A., "Gaussian 94 (Revision C.2)," Gaussian, Pittsburgh, PA, 1995.
44. Peng, C., Ayala, P. Y., Schlegel, H. B., and Frisch, M. J., *J. Comp. Chem.* **17**(1), 49 (1996).
45. Peng, C., and Schlegel, H. B., *Israel J. Chem.* **33**, 449 (1993).
46. González, C., and Schlegel, H. B., *J. Phys. Chem.* **94**, 5523 (1990).
47. González, C., and Schlegel, H. B., *J. Chem. Phys.* **90**(4), 2154 (1989).
48. Levine, I. N., "Quantum Chemistry," Prentice–Hall, Englewood Cliffs, NJ, 1991.
49. Fubini, B., Bolis, V., Cavenago, A., Garrone, E., and Ugliengo, P., *Langmuir* **9**, 2712 (1993).
50. Cortes, J., Jensen, M., and Araya, P., *J. Chem. Soc. Faraday Trans. 1* **82**, 1351 (1986).

51. Mallison, P. D., and McKean, D. C., *Spectrochim. Acta* 30A **1133**, (1974).
52. Barnes, A. J., and Hallam, H. E., *Trans. Faraday Soc.* **66**, 1920 (1970).
53. Acosta Saracual, A. R., Pulton, S. K., and Vicary, G., *J. Chem. Soc. Faraday Trans. 1* **78**, 2285 (1982).
54. Ballard, L., and Jonas, J., *Langmuir* **12**, 2798 (1996).
55. Zhidomirov, G. M., and Kazansky, V. B., *Adv. Catal.* **34**, 131 (1986).
56. Sauer, J., *Chem. Rev.* **89**, 199 (1989).
57. Sauer, J., Ugliengo, P., Garrone, E., and Saunders, V. R., *Chem. Rev.* **94**, 2095 (1994).
58. Chung, J. S., and Bennett, C. O., *J. Catal.* **92**, 173 (1985).
59. Barnes, A. J., and Hallam, H. E., *Trans. Faraday Soc.* **66**, 1932 (1970).
60. Kalasinsky, V. F., and Anjaria, H. V., *J. Phys. Chem.* **84**, 1940 (1980).
61. Barnes, A. J., Hallam, H. E., and Jones, D., *Proc. R. Soc. London A* **335**, 97 (1973).